In-Situ Observation of the Structure of Crystallising Magnesium Sulfate Heptahydrate Solutions with Terahertz Transmission Spectroscopy

Q. Li,[†,‖] J. Kölbel,[†,‖] M. P. Davis,[‡] T. M. Korter,[‡] A. D. Bond,[¶] T. Threlfall,[§] and J. A. Zeitler[*,†]

†*Department of Chemical Engineering, University of Cambridge, Cambridge, CB3 0AS, UK*

‡*Department of Chemistry, Syracuse University, Syracuse, NY, USA*

¶*Yusuf Hamied Department of Chemistry, University of Cambridge, Lensfield Road, Cambridge, CB2 1EW, UK*

§*Department of Chemistry, University of Southampton, Southampton, SO17 1BJ, UK*

‖*Contributed equally to this work*

E-mail: jaz22@cam.ac.uk

Phone: +44 (0) 1223 334783. Fax: +44 (0) 1223 334796

Abstract

Terahertz time-domain spectroscopy in a transmission geometry combined with visual analysis was used to investigate the crystallisation process of $MgSO_4$ solution. Careful spectral analysis of both a feature at 1.6 THz and the baseline allowed the extraction of information about the liquid phase before and during crystallisation, aiding the investigation of solvation dynamics and the behaviour of molecular species at phase

boundaries. The method was reproducibly applied to a number of measurements on a series of solutions of three chosen concentrations at different temperatures. When increasing temperature at the end of the measurement, the dissolution of crystals was observed as well. The temperature-dependent absorption data of the semi-crystalline systems were converted to the solvent concentrations using a recently developed method. Solutions of a series concentrations were also investigated in the temperature range of 4 °C to 25 °C. The results were compared to the theoretical calculated values, and the consistent differences proved the existence of a hydration shell around the salt ions whose behaviour is different from bulk water. Future work will focus on triggering nucleation at specific positions in order to study the very beginning of the crystallisation process. $MgSO_4$ heptahydrate is used as a model system in this study, while the concept and the set-up can be applied to other systems.

Introduction

The crystallisation process has been used for centuries as a purification and separation step for various applications. Therefore, it is surprising that empirical models rather than fundamental understanding still govern the comprehension of crystallisation's underpinning mechanisms and kinetics. What is well established is that nucleation and crystal growth are the two main steps contributing to the crystallisation process. However, the microscopic mechanism of the formation of the nuclei and how they subsequently evolve into crystals is still unclear .[1–4] Two widely popular models are used to describe the crystallisation process: classical nucleation theory and non-classical theory. The former states that density and order fluctuations in the solution cause the formation of crystal-like clusters, which in turn result in nuclei that gradually grow into the crystal form defined by the packing of the cluster.[5] The non-classical theory proposes that the clusters first formed are liquid like, and crystalline order is only introduced later when they grow into nuclei.[6,7]

One widely used model system for investigating crystallisation is the $MgSO_4$-H_2O system.

A variety of hydrate forms can crystallise depending on the temperature and concentrations in solution, but this system also recently received added attention because the presence of such sulfates and their hydrated forms are discussed as the origin of near-surface water content on Mars.[8] A comprehensive understanding of the crystallisation mechanism is highly desirable to support further research into this topic.

A range of techniques are widely used to investigate the crystallisation process: Traditional crystallographic methods to characterise crystalline structures, such as small-angle and wide-angle X-ray scattering, X-ray spectroscopy, and X-ray diffraction; spectroscopic techniques including nuclear magnetic resonance (NMR), Fourier-transform infrared spectroscopy (FTIR), and Raman spectroscopy provide insight into the chemical structure and the shape of the molecules during crystallisation; ultraviolet-visible (UV-Vis) spectroscopy can measure the solute concentration but are of limited use when nascent particles result in scattering losses that cannot be distinguished from absorption.[3,9] Turbidimetry is used to measure the loss of intensity of transmitted light due to the scattering effect of those particles. Second-harmonic generation and polarised light microscopy are applied to detect the onset of crystallisation but are not very sensitive to the structure.[10,11]

When investigating crystallisation in aqueous solutions, the strong absorption due to the presence of water makes it impossible to perform FTIR measurements in transmission. Instead, observations are restricted to surface measurements using attenuated total reflection (ATR). While Raman spectroscopy does not suffer from this restriction, the lack of interaction means that only very little information, if any, of the solvent molecules during the crystallisation process can be extracted.[12]

Terahertz time-domain spectroscopy (THz-TDS) offers a unique perspective to characterise the crystallisation process both in terms of information from the solvent as well as the emerging crystals. By measuring the amplitude and phase of single-cycle pulses of far-infrared radiation, in solution, THz-TDS can probe large-amplitude inter-molecular vibrations as well as high-frequency dielectric relaxation processes that correspond to relaxation

times of less than 10 ps.[13] In solids, the technique can distinguish between different polymorphic forms, cocrystals, hydrates and solvates, as well as provide an excellent measure for overall crystallinity and defect density crystallinity since the long-range order in crystals results in well-defined spectral features (fingerprints) in the terahertz region. In contrast, in amorphous materials, the lack of long-range order results in the collapse of the well-defined peaks into a vibrational density of states (VDOS), which starts at a few hundred gigahertz and exceeds the entire spectral bandwidth of modern THz-TDS spectrometers (0.3 THz to 3 THz). It is characterised by a featureless, monotonously increasing absorption coefficient that typically peaks at frequencies beyond 3 THz.[14]

The deconvolution of individual atomic contributions in experimental terahertz spectra is not possible without additional information, which is usually gathered from theoretical simulations. Density functional theory (DFT) simulations provide normal mode vectors and force constants and can therefore be used to investigate and visualise vibrational modes.[15]

Studies of water and water/alcohol mixtures with THz-TDS suggested key concentration transition points that marked different stages of water and alcohol molecular interactions.[16] Other water mixtures and solutions also demonstrated the use of THz-TDS to probe water molecules based on their mobilities and the behaviour of the hydration shell.[17,18] As well as for characterising static structures, THz-TDS has also been found useful to probe reaction dynamics, such as solid-solid phase transitions, amorphous-solid transformations, and crystallisation.[13,19–21]

Previously, terahertz spectroscopy has been applied to study the crystallisation of sugar and L-(+)-tartaric acid utilising attenuated total reflectance geometry and triggering the crystallisation process by the evaporation of water from the aqueous solution.[20,21] During crystallisation the VDOS is depleted, resulting in the emergence of peaks and a dropping of the overall baseline given its nature as the flank of the VDOS. THz-TDS can therefore simultaneously probe amorphous and crystalline phases represented by the behaviour of the baseline and peaks, respectively. In addition, this suggests that the behaviour of liquid

phase can be extracted explicitly from the baseline while crystallising, hence the solute concentration can be measured even in semi-crystalline samples.[22]

$MgSO_4$ is chosen as a model system to demonstrate that THz-TDS is an option to complement the currently widely applied tools in the field of crystallisation. The versatile set-up based on THz-TDS in transmission geometry and the methodology described in detail in Li et al.[23] and Kölbel et al.[22] is further used to observe the dissolution of crystals at elevated temperatures, calculate the equivalent local concentration, and can be extended to other systems of interest.

Methods

Solid-state samples measurements

Commercial samples of four different $MgSO_4$ hydrates were investigated (as listed in Table S1 in SI). Powder X-ray diffraction measurements were made on a Panalytical XPert Pro diffractometer in Bragg-Brentano geometry using non-monochromated CuKα radiation ($\lambda_{\text{ave}} = 1.5418\,\text{Å}$). Samples were prepared on glass flat-plate sample holders, and data were measured over the range $2\theta = 5°$ to $70°$ with an effective step size of $0.0167°$ and counting time of 60 s per step. Measured data were compared to simulated patterns generated using Mercury[24] from available crystal structures of $MgSO_4$,[25] $MgSO_4 \cdot H_2O$[26] and $MgSO_4 \cdot 7H_2O$.[27]

For terahertz measurements, the crystalline samples were ground gently in an agate mortar with a pestle, and the polycrystalline samples were then mixed with polyethylene (Induchem, Volketwil, Switzerland) to a defined concentration that varied for different hydrates, as detailed in Table S1 in the SI.

The well-mixed powder was compressed into a pellet of 13 mm diameter with a thickness of 2 mm to 3 mm using a hydraulic press (Specac Ltd., Kent, UK) at a load of 2 ton, and a blank polyethylene pellet prepared in the same way was used as a reference. During the THz-TDS transmission measurement, 1000 waveforms were acquired and averaged, with a

resolution of $0.94\,\mathrm{cm}^{-1}$.

Additionally, a supersaturated solution of $MgSO_4$ was prepared from $MgSO_4$ heptahydrate 98 % (Sigma-Aldrich, Gillingham, UK) dissolved in Milli-Q water (IQ 7000, Merck, Darmstadt, Germany, resistivity $18.2\,\mathrm{M\Omega \cdot cm}$), and filled into a well-sealed petri dish. The petri dish was left in a fume hood at 20 °C until crystals formed. This process was to mimic the crystallisation process in the crystallisation cell. Due to constraints of the set-up it was impossible to investigate crystals grown directly in the microfluidic cell at cryogenic temperatures. The crystals grown in the petri dish were made into pellets using the method described above and characterised at cryogenic temperatures with terahertz spectroscopy later to confirm their structure more accurately.

THz-TDS measurements were performed with a commercial spectrometer TeraPulse 4000 (TeraView Ltd., Cambridge, UK), and the measurement chamber was purged with nitrogen to eliminate the effect of water vapour. Variable-temperature measurements were facilitated by a cryostat (Janis, Massachusetts, USA) and the temperature was well-controlled with an attached temperature controller Lakeshore 330 (Ohio, USA). The sample pellets were first cooled down to 80 K and then heated up in steps to 300 K to examine the temperature-dependent behaviour of the spectral features. Measuring commercial samples at room temperatures allows the direct comparison of their spectra with those acquired during crystallisation experiments. However, acquiring spectra for crystalline samples at lower temperatures improves their quality since absorption in the terahertz region is highly affected by the temperature background, reflected in effects such as peak broadening and peak shifting.

Computational Methods

The solid-state density functional theory (ss-DFT) program CRYSTAL17 [28] was used to perform geometry optimisation and frequency analysis calculations on $MgSO_4$ heptahydrate. All calculations utilised the revised version of the Peintinger-Oliverira-Bredow split-valence triple-ζ basis set (pob-TZVP-rev2) [29] and the Becke-3-Lee-Yang-Parr (B3LYP) [30,31] hybrid

density functional. The B3LYP density functional was supplemented with Grimme's non-covalent dispersion correction (D3) and the Becke-Johnson damping correction[32–34] with three-body Axilrod-Teller-Muto repulsion contributions (program keyword "ABC").[35–37] In all $MgSO_4$ heptahydrate calculations, 125 k-points were used in the irreducible Brillouin zone (keyword SHRINK=9) and 99 radial point and 1454 angular points were used for the pruned integration grid. The overlap-based truncation criteria for the bielectronic integrals (Coulomb and exchange) (program keyword "TOLINTEG") were set to 10^{-12}, 10^{-12}, 10^{-12}, 10^{-20} and 10^{-40} for all calculations and the maximum order of multipolar expansion was set to 6 (program keyword "POLEORDR"). The starting structure for $MgSO_4$ heptahydrate was published by Ferraris, Jones, and Yerkess in 1973[27] and the initial ionic charges were explicitly set to Mg^{2+} and $(SO_4)^{2-}$. In the geometry optimisation, the lattice dimensions and atomic positions were allowed to fully optimise within the $P2_12_12_1$ space group, and the energy convergence was set to $\Delta E < 10^{-8}\,E_\mathrm{h}$. The optimised structure was used to calculate the vibrational frequency analysis and the energy convergence was set to $\Delta E < 10^{-10}\,E_\mathrm{h}$. The vibrational frequency analysis determined that the optimised structure was a minimum on the potential energy surface (no negative frequencies). During the frequency analysis, each atom was displaced twice along each Cartesian axis and the numerical derivatives of the Hessian matrix were calculated using the central difference formula. The IR intensities were calculated using the Berry phase method.[38,39]

Crystallisation measurements

To investigate crystallisation, magnesium sulfate solutions were prepared at various concentrations using commercial $MgSO_4$ heptahydrate 98 % (Sigma-Aldrich, Gillingham, UK). The sample was dissolved in Milli-Q water (IQ 7000, Merck, Darmstadt, Germany, resistivity $18.2\,\mathrm{M\Omega \cdot cm}$) in a beaker, which was then left on a magnetic stirrer until the crystals were fully dissolved. After several rounds of preliminary experiments, three concentrations (mass ratio of $MgSO_4$ heptahydrate to water) were chosen for further repeats: 1.41:1, 1.29:1, and

1.20:1. This was based on the time and temperature observed for crystallisation.

A detailed description of the crystallisation set up was given in an earlier paper.[23] The set up consisted of a liquid cell that was held by a hollow metal sample holder inside of which water was circulated. The temperature of the circulating water was controlled via an external water bath, whose temperature was balanced between an electric heater and the surrounding ice bath with an accuracy of 0.1 °C. The operation temperature was in the range of 4 °C to 90 °C, and during the experiments described here it was operated between 4 °C to 25 °C.

Air was used as the reference, and the high-resolution mode of the spectrometer was utilised to extend the extent of acquired time-domain waveforms to 45 ps. Each spectrum was formed of the average of 15 individual waveforms with a spectral resolution of 0.94 cm^{-1}, resulting in an acquisition time of 20 s per spectrum. The valid frequency range was from 0.35 THz to 2 THz.

When monitoring the crystallisation process at a set temperature, the cell was first cooled down and kept constant at the target temperature until the system was stable. Afterwards, the $MgSO_4$ solution was injected into the flow cell with a syringe via a tube, and the outlets on both sides of the flow cell were sealed with parafilm. The sample holder including the cell was promptly placed at the centre of the measurement chamber and terahertz spectra and images were acquired. The time from injecting the solution to the start of the measurement was minimised to no more than 30 s, in case of triggering undesired nucleation. The temperature was kept as constant as possible during the whole crystallisation process, until crystals formed across the cell in the view of the optical probe and the terahertz spectra did not exhibit further changes. The experiment was either terminated at this point, or the behaviour of the system during slow heating to room temperature was studied. In the latter case, the temperature was increased by 0.2 °C min^{-1} up to 25 °C in the flow cell. This was found to be an ideal heating rate to introduce a constant temperature change to the cell.

For all measurements, three thermocouples monitored the temperature at various posi-

tions: in the water bath, inside the metal sample holder, and at the inlet of the cell, and one data point was acquired per second. The optical probe used for image acquisition was set to acquire one photograph every two seconds. After each crystallisation measurement, the liquid cell was thoroughly cleaned to remove grown crystals, contaminations, or seeds which could influence subsequent measurements. The cleaning solution was prepared from commercial EDTA solution (pH = 8; Fisher Scientific, Loughborough, UK) and NaOH solution (Reagecon Diagnostics, Shannon, Ireland) to adjust the pH to 10 in which $MgSO_4$ exhibits a higher solubility.

Results and Discussion

PXRD analysis of $MgSO_4$ hydrates

Commercially available samples of anhydrous $MgSO_4$ from two different suppliers and the $MgSO_4 \cdot 7H_2O$ sample were highly crystalline and agreed closely with the patterns simulated from the crystal structure.[25,27]

The $MgSO_4 \cdot H_2O$ sample showed much broader peaks, indicative of smaller particle/domain size. It largely agreed with the pattern simulated from the monohydrate crystal structure,[26] but additional peaks at $2\theta \approx 20°$, 32° and 40° (marked by an asterisk in Figure S2 in the SI) indicate the presence of an additional minor phase. Comparison to other known $MgSO_4/H_2O$ phases suggests the impurity was most likely to be hexahydrate:[40] its most prominent peak matched that seen at $2\theta \approx 20°$, plus groups of peaks just above 30 ° 2θ and just below 40 ° 2θ could match to the features seen in the monohydrate sample.

All measured and simulated PXRD patterns can be found in the supporting information.

Terahertz spectra of $MgSO_4$ hydrates

The terahertz spectra of $MgSO_4$ anhydrous, monohydrate, heptahydrate, and the crystal grown in the lab from solution were acquired at different temperatures (Figure 1). Comparing

the spectra of the three different hydrates, neither the anhydrous nor monohydrate forms of $MgSO_4$ showed pronounced peaks in the region of interest (0.3 THz to 3.0 THz), and the only change that was observed upon cooling was a drop in the baseline.

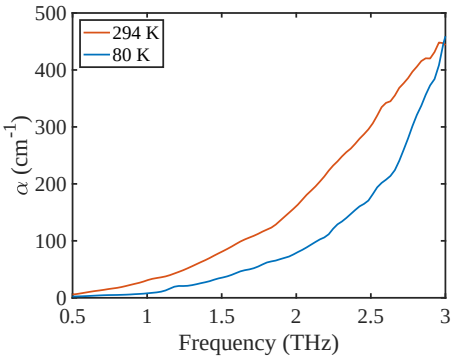

(a) Anhydrous $MgSO_4$.

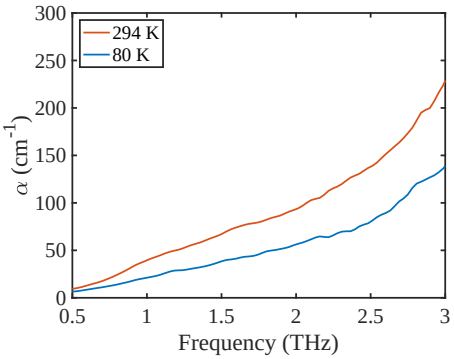

(b) $MgSO_4$ monoydrate.

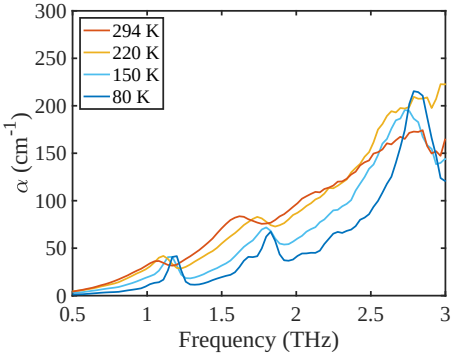

(c) Commercial $MgSO_4$ heptahydrate.

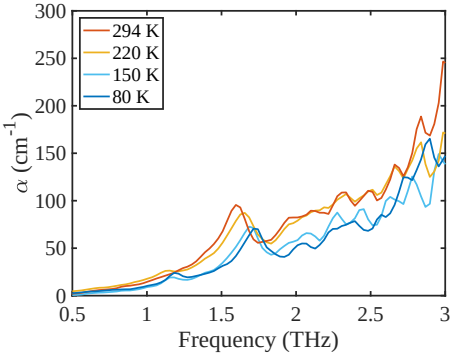

(d) $MgSO_4$ heptahydrate grown in the lab from solution.

Figure 1: Crystalline $MgSO_4$ hydrates measured at different temperatures.

For the commercial heptahydrate sample, three pronounced bands were observed at 80 K: at 1.2 THz, 1.7 THz (double features), and 2.8 THz. These vibrations probably resulted from the interactions between $MgSO_4$ and water because they were not present in the anhydrous and monohydrate samples. As expected, the spectra exhibited peak broadening and shifting as well as an increase of the baseline upon heating to room temperature. This is due to the significant population of excited vibrational states at room temperature, which is characteristic of the far-infrared where the energy gap between ground state and excited states is lower than in the infrared. In addition, the increased thermal vibration and emission contribute to

this effect. At 294 K, which was close to the temperature of the crystallisation experiments, the high intensity peak at 2.8 THz diminished into the baseline and the two features at lower frequencies became weaker and broader while the double peak at 1.7 THz merged and shifted to a single feature at 1.6 THz.

The spectra of crystals grown under the conditions similar to the crystallisation in the flow cell exhibited less temperature-dependent behaviour. The feature at 1.2 THz was slightly more intense at low temperatures, while the peak at 1.7 THz was consistently observable in the whole temperature range. The latter shifted to 1.6 THz upon heating to room temperature, though as a single feature rather than a double one at temperatures above 80 K. The high similarity between the terahertz spectra of heptahydrate and grown crystals, especially at 294 K, confirmed that the crystals grown in the crystallisation cell were indeed $MgSO_4$ heptahydrate. The differences between the two could be accounted for by the different purity and defect density. In addition, the 1.1 THz peak became too weak to be observed at room temperature, so the feature at 1.6 THz was used in the following analysis to monitor the crystallisation process.

Within the inherent limitations of the computational methodology[41] the ss-DFT simulation produced a very good correlation with the experimental results (see Figure 2). The relative shift in the frequencies of the features between calculation and experiment is expected due to the difference in temperature between calculation and the experimental data amongst other factors. No scaling was applied to the frequency of the calculated modes. The calculation revealed that the double features near 1.7 THz originate from three distinct lattice vibrational motions predicted to be at 1.74 THz, 1.93 THz and 1.96 THz. As outlined above, the slight overestimation of the vibrational frequencies is attributable to the simulation being performed at 0 K while the experimental data is acquired at temperatures ≥ 80 K. The predicted 1.74 THz vibration (B3 symmetry) involves primarily the rotational motions of the $[Mg(H_2O)_6]^{2+}$ and $(SO_4)^{2-}$ moieties about the *c*-axis of the crystallographic unit cell, with a smaller contribution of translational motion along the *a*-axis. The 1.93 THz vibra-

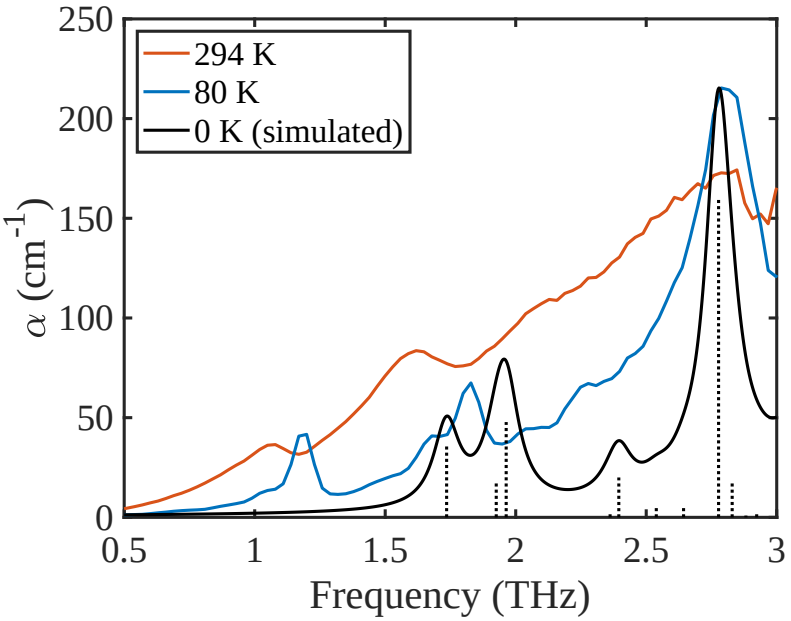

Figure 2: Comparison of simulated (black) and measured spectra of $MgSO_4$ heptahydrate. Simulated data have been scaled to the feature at 2.8 THz. Dotted lines denote positions and relative intensities of infrared-active modes.

tion (B3 symmetry) is a translational vibration of the crystal components along the *c*-axis. The 1.96 THz mode (B2 symmetry) is largely rotational motion like the 1.74 THz mode but with rotation about the *c*-axis and some translational motion along the *b*-axis. The intense experimental peak near 2.8 THz is predicted at 2.78 THz (B3 symmetry) and is a rotational lattice vibration about the *a*-axis with a small component of translation along the *c*-axis. Noticeably missing from the simulation is a feature matching with the experimental peak at 1.2 THz, as the 1.74 THz vibration is the lowest frequency vibration (infrared or Raman) produced by ss-DFT. The reason behind this absence is not clear. The use of other basis sets and density functionals did not produce the lower feature, nor did the explicit calculation of transverse optical (TO) and longitudinal optical (LO) phonon splitting. One possible explanation is that the published space group of $P2_12_12_1$ is not an accurate representation of the symmetry of the crystal at reduced temperatures and is instead $P2_1$ as suggested by others.[42] A reduction in crystal symmetry may yield new vibrations in the ss-DFT predicted spectra, but such simulations are not trivial given the high computational cost of the much

larger asymmetric unit.

Crystallisation of $MgSO_4 \cdot 7H_2O$

As described in the method section, the flow cell was kept constant at the desired temperature for crystallisation, and the process was monitored with both terahertz spectroscopy and an optical probe. Confirmed by visual analysis, crystallisation was usually observed to start at either inlet or outlet (or both) of the crystallisation cell, followed by crystal growth across the cell to its other end. Acquired images were useful complementary information to track the progress of crystal growth throughout the cell. After performing image edge detection and binarisation, crystals were represented by white pixels, and the amount of crystals in the field of view of the camera was quantified as demonstrated in Figure 3. In most measurements, it took approximately 4 min to 10 min for crystals to grow from one end of the cell to the other once crystal growth had initiated.

The spot of terahertz radiation probing the centre of the cell was about 2 mm in diametre (as highlighted in Figure 3(b)). Before the crystals had grown into the centre of the cell, the sample volume probed with terahertz radiation was entirely filled with liquid, and the terahertz spectra were hence completely featureless. However, as crystal growth continued toward the centre of the cell, the absorption below 1.6 THz decreased and a peak emerged at 1.6 THz. This indicated the existence of crystals in the field of view of the spectrometer (see Figure 3(d)). The peak at 1.6 THz correlated with the peak in the solid state heptahydrate samples measured previously and shown in Figure 1. The time by which crystals were detected by THz-TDS coincided well with the time expected from image analysis (also shown in Figure 3(c)).

Three frequencies were chosen to illustrate the changes of the spectrum over the course of the experiment: 1.6 THz, i.e. the peak maximum, 1.0 THz, the frequency where the spectrometer has the highest signal to noise ratio, and 0.5 THz, which was a sufficiently low frequency that it should not directly be influenced by the crystalline spectral feature. At

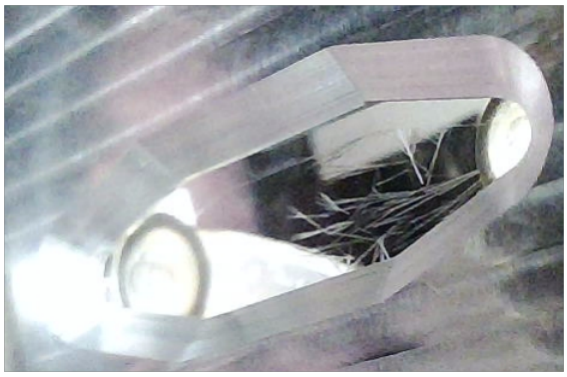

(a) Raw image recorded when the crystals grew into the middle of the cell and were detected by THz-TDS.

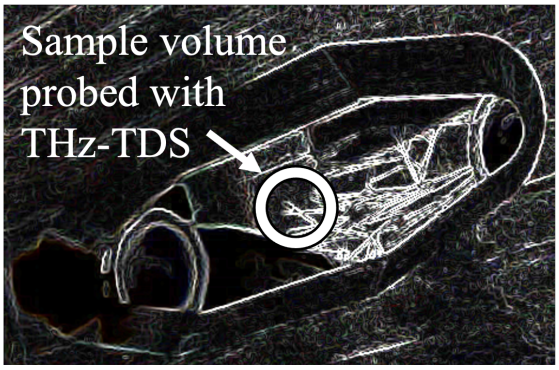

(b) 3(a) after edge detection. The approximate sample volume probed with THz-TDS is highlighted.

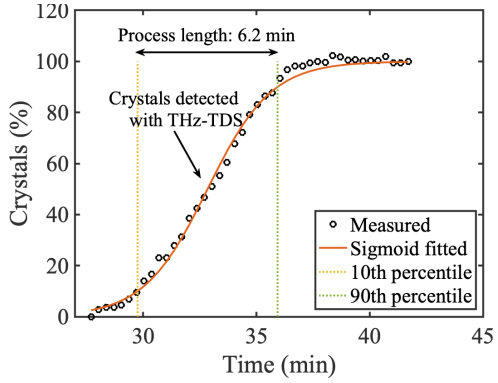

(c) Percentage of area covered by crystals as observed with visual analysis plotted against time. In this case, the crystal growth through the cell occurred in about 6 min at around 4 °C.

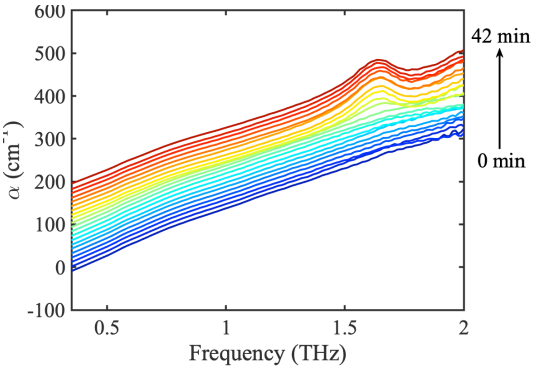

(d) Terahertz spectra acquired during crystallisation. Each subsequent spectrum is offset by $10\,\mathrm{cm}^{-1}$.

Figure 3: Visual analysis of crystal growth.

each of those three frequencies, the absorption coefficient was extracted and plotted as a function of time, as illustrated in Figure 4.

An algorithm was used to differentiate reliably and reproducibly between three regions (before, during, and after crystal growth) by fitting three linear functions to the data and selecting the fits that minimised the sum of their root mean square error. The fits are in Figure 4. This allowed more information to be extracted at each stage of the crystallisation, and facilitated comparison between the subsequent measurements which were performed under a range of conditions.

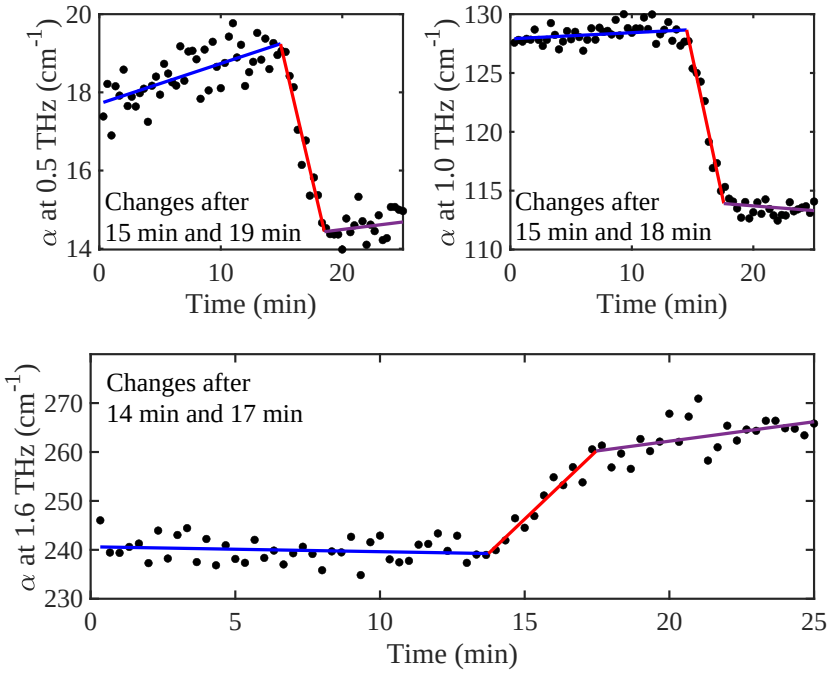

Figure 4: Absorption extracted at 0.5, 1, and 1.6 THz. This highlighted the different behaviour of the peak feature compared to the rest of the spectrum (i.e. the differences between crystalline and liquid phases). Whereas the absorption at 1.6 THz increased after 14 min, when crystallisation occurred, the absorption decreased at lower frequencies. Linear fits were performed before (first region, blue), during (second region, red), and after (third region, purple) crystal growth through the field of view.

Crystallisation experiments and the analysis described above were performed for a range of different temperatures and concentrations. A measure for how fast the crystals covered the field of view was found by evaluating the time difference between the emergence of the peak

and reaching the equilibrium afterward. This time period was denoted as "second region". The "first region" corresponded to the time before crystals appeared in the field of view, and the "third region" referred to the last part of the experiment after crystals had fully covered the field of view.

During analysis, the slope of the linear fit to the data points in the second region was evaluated. In most experiments, the gradient of the linear fit was positive for 1.6 THz and negative at lower frequencies.

Figure 5(a) clearly shows the different behaviour of the absorption for the peak at 1.6 THz compared to other frequencies. While the absorption at 1.6 THz (triangles) increased during crystallisation, it decreased for lower frequencies (dots and diamonds). The spread was higher at higher concentrations, meaning that a faster crystallisation was more likely to result from more supersaturated solutions of $MgSO_4$.

If less time was spent in the second region, i.e. the crystal growth rate was increased, the higher was the absolute gradient in that region at all frequencies. This was shown in Figure 5(b). For better clarity, the slope during the phase at which the crystals grew into the field of view of the THz-TDS system was shown at only 1 THz, where the signal to noise ratio was largest. The slope in the second region of the data at 1 THz was plotted against the time the crystals took to fully cover the field of view of the spectrometer. The shown slope was negative because the absorption decreased at 1 THz when crystals appeared.

Figure 5(c) shows the relationship between the duration of the middle region with the temperature at which the experiments were performed. While crystal growth through the field of view of the spectrometer seemed to take around 4 min at temperatures between 3.5 °C to 5 °C, the spread was larger at temperatures above 6 °C. In one extreme case it took almost 40 min for the crystals to fully cover the field of view. In most other cases, it took between 2 min to 12 min, independent of concentration. Finally, Figure 5(d) shows how much the absorption at 1.0 THz changed with time at different temperatures and concentrations.

Combining Figure 5(a) and Figure 5(c) it was concluded that, based on the results from

our experiments presented here, both a higher initial concentration and elevated temperature above 6 °C made the crystal growth more erratic indicated by a wider spread of the data.

Calibrated local concentration and hydration shell

Terahertz spectra are inherently temperature dependent. As discussed above, both a decrease in $MgSO_4$ concentration and an increase in temperature yield a higher absorption coefficient. Therefore, if the data are corrected for temperature variations, all changes that are observed in the absorption coefficient are directly linked to structural changes of probed sample volume.

To eliminate temperature effects, a calibration procedure previously established[22] was followed. By measuring the absorption of liquid mixtures of varying concentrations at different temperatures, a calibration curve had previously been determined. This allowed the calculation of the concentration of a solution of unknown concentration at arbitrary temperatures. In purely liquid samples, the calibration procedure resulted in the actual concentration for solutions. However, the emergence of crystalline features affected the spectra and in this case, the liquid phase absorption was calculated at frequencies furthest away from the peak of the crystalline feature at 1.6 THz.

An example of converting temperature-dependent data into the temperature-independent equivalent concentration is shown in Figure 6. Instead of the slowly rising absorption before crystals reached the field of view that was observed in Figure 4, the concentration decreased. This complemented the information gained only by analysing the absorption coefficient and yielded an explanation of the changes in the spectra during crystallisation as follows.

At the beginning of the experiment, both the terahertz spectra and visual analysis confirmed the absence of $MgSO_4$ crystals located in the centre of the cell. Once nucleation occurred, typically not in the centre of the cuvette but near one end of the cell, a local increase in water concentration was observed in the terahertz spectra due to the increase in water concentration immediately adjacent to the growing crystals as magnesium and sul-

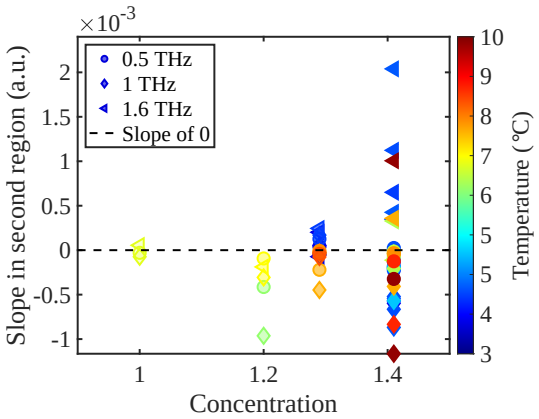

(a) Slope in the second region plotted against concentration, shown at 0.5 THz (dots), 1.0 THz (diamonds), and 1.6 THz (triangles). The colour denotes the temperature at which the system was kept during crystallisation.

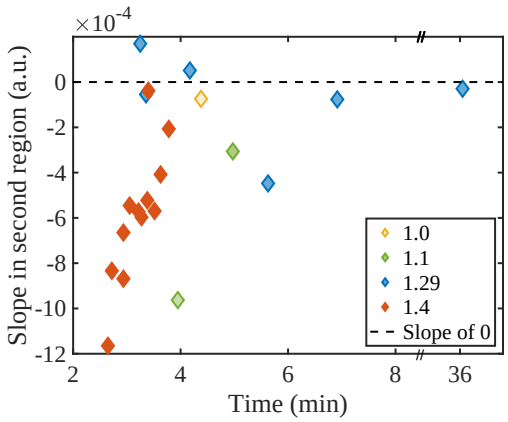

(b) Gradient of the linear fit to the absorption at 1.0 THz in the second region plotted against time. The colour denoted the different initial concentrations.

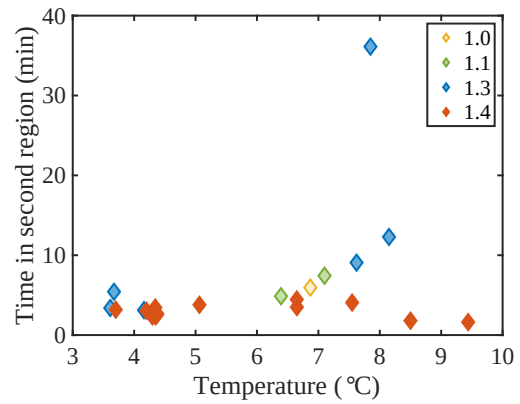

(c) Time spent in the second region plotted against temperature. The data was extracted at 1.0 THz and different colours denoted different initial concentrations.

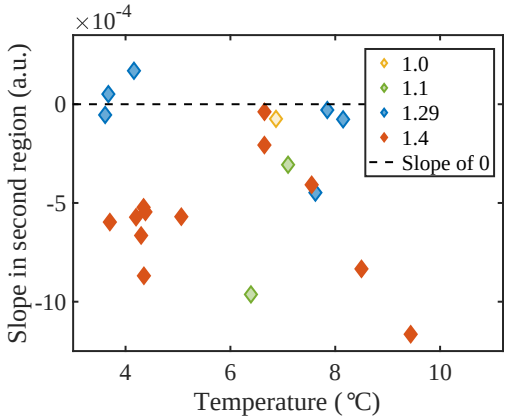

(d) Slope in the second region plotted against the temperature at which the experiments were performed, shown at 1.0 THz and different colours denoted different initial concentrations.

Figure 5: Analysis parameters during crystal growth plotted against concentration, time, and temperature. The concentrations were represented by the mass ratio of $MgSO_4$ heptahydrate to water.

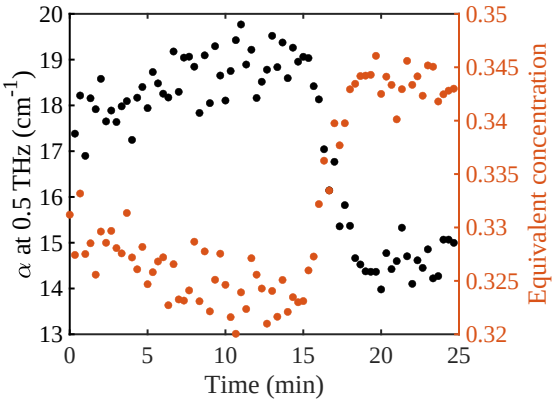

(a) Absorption α at 0.5 THz (black) and corresponding calculated liquid phase solute concentration over time (red).

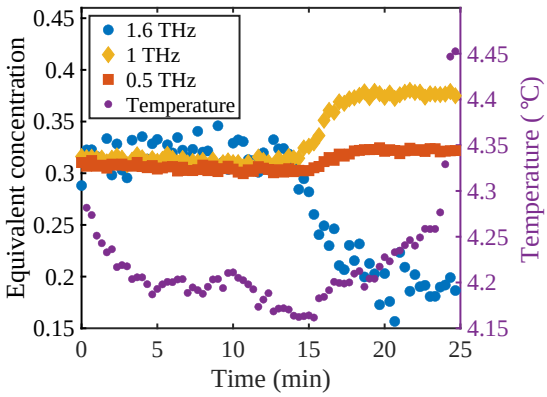

(b) Liquid phase solute concentration calculated at 0.5 THz (red squares), 1.0 THz (orange diamonds), and 1.6 THz (blue dots). Right: The temperature throughout the measurement. It was stable and stayed within 0.1 °C of the setpoint until the temperature control was turned off after crystallisation.

Figure 6: Illustration of using the calibration method to calculate liquid phase solute concentration based on measured absorption at various frequencies.

phate ions crystallised into the $MgSO_4$ heptahydrate form. This caused a slight increase of the absorption coefficient, corresponding to a lower $MgSO_4$ concentration measured in the centre of the cell.

$MgSO_4$ in solution is surrounded by a hydration shell whose absorption is markedly different from that of bulk water.[43] This was demonstrated by calculating a theoretical absorption coefficient based on the known absorption coefficient of pure water (α_{water}) and that of anhydrous $MgSO_4$ and that of $MgSO_4{\cdot}7H_2O$ (α_{crystal}), neglecting the effect of a larger hydration shell. A series of $MgSO_4$ aqueous solution with a range of concentrations were measured, and a difference between the measured (α_{solution}) and the calculated ($\alpha_{\text{ideal mixture}}$) absorption was consistently observed.

$$\alpha_{\text{ideal mixture}} = \alpha_{\text{crystal}} \cdot c_{MgSO_4} + \alpha_{\text{water}} \cdot c_{\text{water}} > \alpha_{\text{solution}} \tag{1}$$

This difference was calculated with Eqn. 1 for a number of measurements and is shown

in Figure 7 for anhydrous $MgSO_4$, where c_{MgSO_4} represents the molar concentration of anhydrous $MgSO_4$ or $MgSO_4 \cdot 7H_2O$ of the solutions in the corresponding case. Calculated values for both anhydrous $MgSO_4$ and $MgSO_4$ heptahydrate are shown in Table S2 in the SI. Changes were subtle below 0.02 molar concentration and increased steadily above for in both the case of anhydrous $MgSO_4$ and $MgSO_4$ heptahydrate.

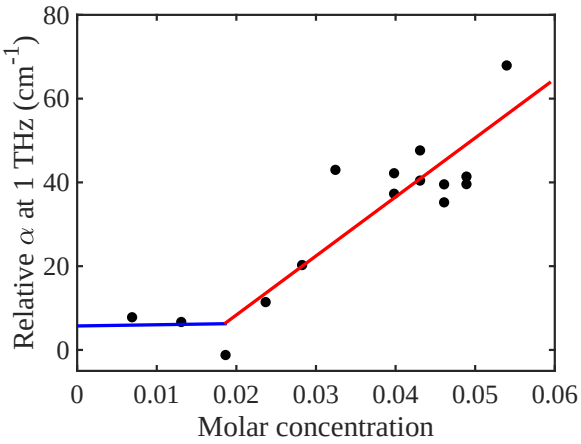

Figure 7: Relative absorption calculated and plotted against molar concentration of $MgSO_4$. The experimental error is on the order of $4\,cm^{-1}$. The lines are drawn to guide the eye and are not intended to be indicative of a physical model.

The calculated theoretical absorption excluding the effect of the hydration shell was larger than that of the measured absorption, indicating that the hydration shell surrounding $MgSO_4$ had a lower absorption coefficient than the bulk water that it replaced which is in line with expectation as the dipoles in the hydration shell tend to exhibit slower relaxation behaviour. The results also inferred that the hydration shell encompassed more than the 7 water molecules that form part of the $MgSO_4$ heptahydrate crystal because of the observed difference between the measured and calculated absorption. This is in line with other observations that also found extended hydration shells when probing samples with THz-TDS.[43]

An increase of the overall absorption coefficient at 0.5 THz and 1.0 THz as seen in experiments when crystals grew hence corresponded to water being expelled from the hydration shells into the bulk phase when the crystals formed. The bulk aqueous phase is pushed toward the field of view sampled by THz-TDS during the growth of the crystals before the

crystals themselves enter the field of view of the terahertz beam. Therefore, the growth of $MgSO_4$ heptahydrate, that started at one end of the cell, increased the local concentration of bulk water in the centre of the cell, where it was probed with THz-TDS. This explained the initial slight increase in absorption that was observed at both 0.5 THz and 1.0 THz, given that the absorption coefficient of bulk water is much higher than that of the solution mixed with $MgSO_4$ or the heptahydrate.

Once the crystals reached the centre of the cell, the absorption at 0.5 THz and 1 THz decreased (see Figure 4) as the probed sample became more ordered and thereby the VDOS was depleted, while the absorption at 1.6 THz increased as the peak emerged. On the other hand, the liquid phase concentration seemed to increase at 0.5 THz and 1.0 THz when crystals started to grow in the field of view of THz-TDS. This was in line with a decrease of the hydration shell size, and a potentially denser liquid in the area of forming crystals that was probed with THz-TDS.[3] The absorption coefficient at the peak at 1.6 THz clearly increased, and this effect was accompanied by a decrease in $MgSO_4$ concentration. Once the crystals covered the centre of the cell and the system reached an equilibrium state, the changes at all frequencies became subtle again.

However, the calculated liquid phase concentration was not quantitatively valid at frequencies close to crystal features, as no rigorous method has yet been developed to systematically account for peak effects to the baseline, and the calibration curve was determined from the experimental data of a series of samples in the liquid phase only.

To examine further the influence of the crystalline feature to the data collected at other frequencies, the previous procedure for calculating concentration was applied inversely, i.e. the known and frequency-independent calculated concentration was used to calculate the equivalent absorption if it was fully liquid (α_{liquid}). Of the three frequencies described here, the data at 0.5 THz were the least affected by the crystalline feature, since that frequency was the furthest away from the feature at 1.6 THz. Therefore, the concentration calculated from it was being used as the basis to calculate α_{liquid}.

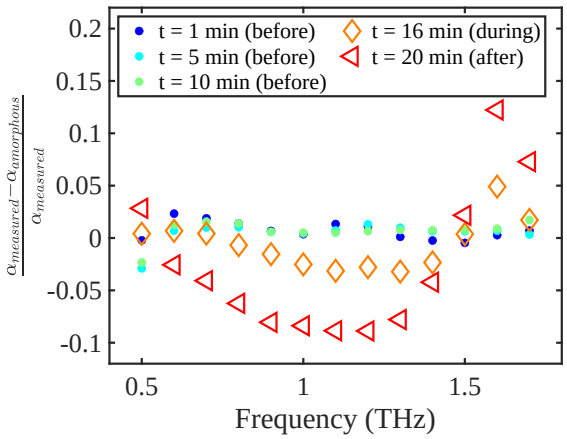

Figure 8: Relative changes in α when comparing the measured to the calculated purely amorphous absorption before, during, and after crystallisation.

The relative difference compared to the measured absorption is plotted in Figure 8 for different experimental stages. Before crystals were observed in the field of view, the relative difference was close to zero for all frequencies. During crystal growth into the field of view however, the relative difference increased between 1.5 THz to 1.7 THz, and decreased between 0.6 THz to 1.4 THz. This effect became even stronger once crystallisation was complete. Maxima of the relative difference were found at 1 THz and 1.6 THz while the difference decreased toward lower frequencies. This showed that while the peak only seemed to impact a relatively narrow frequency range between 1.5 THz and 1.7 THz, the effects of crystallisation are still strongly observed at 1.0 THz. The spectral change was directly visible: depletion of the VDOS below 1.5 THz and appearance of a peak above. It should be noted that while current results focus on crystal growth into field of view of the spectrometer, nucleation itself has not yet been observed directly. This will be the focus of future work, possibly by observing very subtle spectral changes.

Dissolution observed

All the crystallisation experiments were performed and monitored at a constant temperature, and once both visual and spectral analysis confirmed that the crystallisation was completed,

the system was slowly heated up. Meanwhile, it was also observed that crystals started to dissolve at elevated temperatures. Therefore, further measurements were carried out to study this phenomenon systematically.

With the well-controlled heating component, an experimental heating rate of 0.1 °C / 30 s was determined to ensure a constant temperature change in the crystallisation cell. Faster heating might have led to a temperature difference between the circulating water and the inside of the cell, while slower heating rates (although possible) prolonged the experiment. With the chosen heating rate, crystal dissolution was observed within a reasonable experimental time frame. However, an accurate dissolution temperature was not measured because hysteresis effects related to kinetics of crystallisation and dissolution have to be taken into account.

The temperature profile over time is shown in Figure 9(a), and the times when characteristic changes occurred in the spectra are highlighted with vertical lines. These agreed well with the times extracted from the images acquired by the camera. When the temperature was increased steadily once crystals grew completely, crystal dissolution was observed both visually as the percentage of crystals decreased drastically in the cell (Figure 9(c)), as well as with THz-TDS resulting in the disappearance of the crystalline feature at higher temperatures (Figure 9(b)). This was also investigated by utilising the calculation of liquid phase concentrations to remove the temperature effect from the spectra (Figure 9(d)).

The calculated concentration stayed mostly constant once crystals had formed until around 130 min after the beginning of the experiment, which coincided with the first observation of crystal dissolution in the camera images. Because heat was constantly being added to the system by the heat of dissolution of magnesium sulfate and the temperature increased steadily, the equilibrium concentration of $MgSO_4$ in the vicinity of the crystal features varied because the saturation point changed with temperature. Therefore, the crystals dissolved slowly while the surrounding liquid was approaching the point of local saturation upon increasing the temperature. Opposite to crystal growth, dissolution resulted in an

enlargement of the hydration shells accompanied by an increase of the absorption at 0.5 THz and 1.0 THz and a decrease at 1.6 THz. The calculated concentration however decreased at 0.5 THz.

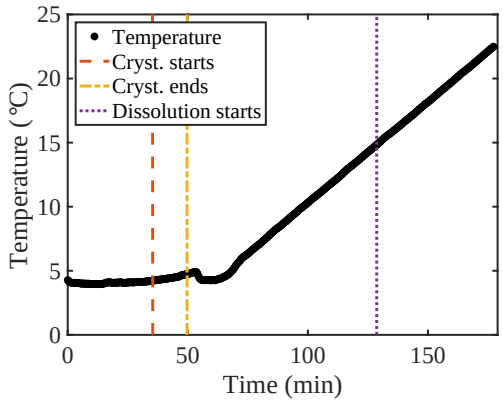

(a) Temperature profile during the experiment. Vertical lines denote changes in the spectra.

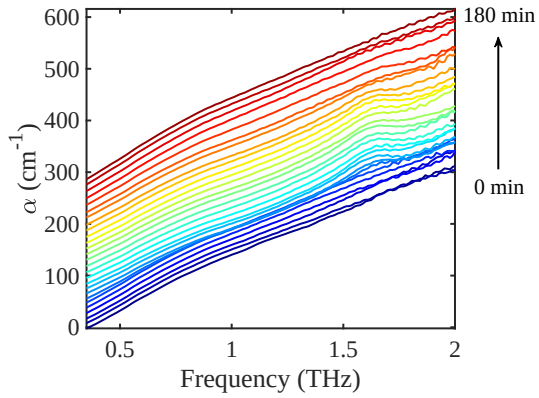

(b) Terahertz spectra acquired throughout the experiment (liquid - semi-crystalline - liquid). Subsequent spectra are offset by 10 cm^{-1}.

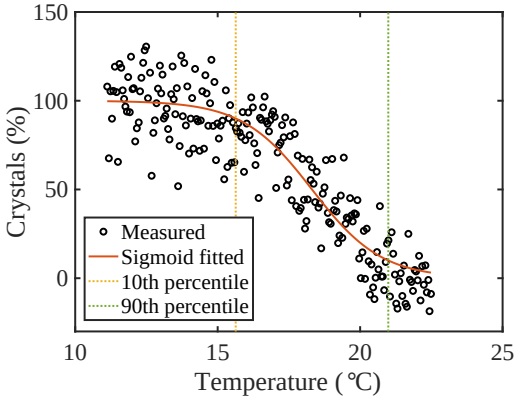

(c) Dissolution of crystals observed with visual analysis. Dissolving started at a temperature shortly below 16 °C and was completed just above 20 °C. At a heating rate of 0.1° / 30 s, this process took about 34 min to complete.

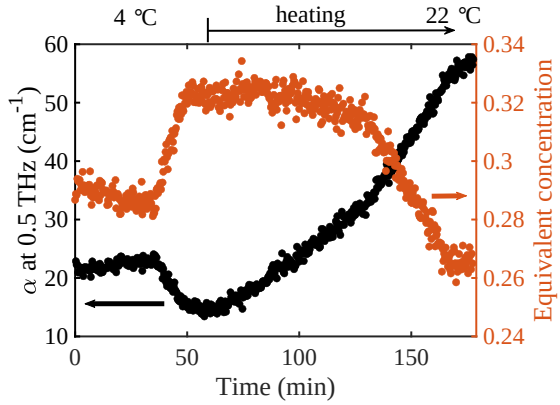

(d) α at 0.5 THz and corresponding calculated concentration over time. After initial crystallisation, the temperature was steadily increased up to room temperature.

Figure 9: Crystal dissolution analysis.

Conclusion

THz-TDS was used to study the crystallisation process of $MgSO_4 \cdot 7H_2O$. The emergence and disappearance of the spectral feature at 1.6 THz indicated the growth or dissolving of crystals in the field of view of the spectrometer (validated by image analysis), while the change of the baseline reflected the behaviour of solvent. This is useful for investigating solvation dynamics and the behaviour of molecular species at phase boundaries.

The absorption at three frequencies was investigated in particular, and the process clearly showed three stages. Experiments at three concentrations and in the temperature range of 4 °C to 9 °C suggested that both a higher initial concentration and elevated temperature above 6 °C were likely to result in a more erratic crystal growth. The faster the crystals grew through the field of view of the spectrometer, the higher was the change in absorption at all frequencies. The temperature effect on terahertz spectra was addressed as outlined previously [21], leading to the calculation of an equivalent liquid phase concentration. In addition, changes in the absorption coefficient were correlated with the composition and size of the hydration shell surrounding the salt ions.

The results covered here are from experiments where the crystals grew into an area probed by terahertz radiation. Therefore, the onset of nucleation was not observed directly. The focus of on-going work is to trigger nucleation at desired locations (e.g. in the centre of the cell) so that the investigation can be extended from that of crystal growth to that of nucleation. The current setup is designed for operating temperatures between 4 °C to 9 °C, and this range can be extended further with simple adjustments. Therefore, this technique can be applied to investigate a wide range of crystalline and semi-crystalline systems, thereby offering an interesting perspective of low-frequency motions of multiphase systems.

Acknowledgement

JK thanks the EPSRC Cambridge Centre for Doctoral Training in Sensor Technologies and Applications (EP/L015889/1) and AstraZeneca for funding. QL thanks the Chinese Scholarship Council for funding. M.P.D. and T.M.K. thank the ITS Research Computing team at Syracuse University for providing computational resources.

References

(1) De Yoreo, J. J.; Gilbert, P. U. P. A.; Sommerdijk, N. A. J. M.; Lee Penn, R.; Whitelam, S.; Joester, D.; Zhang, H.; Rimer, J. D.; Navrotsky, A.; Banfield, J. F.; Wallace, A. F.; Michel, F. M.; Meldrum, F. C.; Cölfen, H.; Dove, P. M. Crystallization by particle attachment in synthetic, biogenic, and geologic environments. *Science* **2015**, *349*.

(2) Desiraju, G. R. Crystal engineering: from molecule to crystal. *Journal of the American Chemical Society* **2013**, *135*, 9952–9967.

(3) Davey, R. J.; Schroeder, S. L. M.; ter Horst, J. H. Nucleation of organic crystals—a molecular perspective. *Angewandte Chemie International Edition* **2013**, *52*, 2166–2179.

(4) Svärd, M.; Devi, K. R.; Khamar, D.; Mealey, D.; Cheuk, D.; Zeglinski, J.; Rasmuson, Å. C. Solute clustering in undersaturated solutions–systematic dependence on time, temperature and concentration. *Physical Chemistry Chemical Physics* **2018**, *20*, 15550–15559.

(5) Volmer, M. *Kinetics of phase formation*; 1939.

(6) Vekilov, P. G. Nucleation. *Crystal Growth Design* **2010**, *10*, 5007–5019.

(7) Gebauer, D.; Cölfen, H. Prenucleation clusters and non-classical nucleation. *Nano Today* **2011**, *6*, 564–584.

(8) Vaniman, D. T.; Bish, D. L.; Chipera, S. J.; Fialips, C. I.; William Carey, J.; Feldman, W. C. Magnesium sulphate salts and the history of water on Mars. *Nature* **2004**, *431*, 663–665.

(9) Ojeda, C. B.; Rojas, F. S. Process analytical chemistry: applications of ultraviolet/visible spectrometry in environmental analysis: an overview. *Applied Spectroscopy Reviews* **2009**, *44*, 245–265.

(10) Correa-Soto, C.; Trasi, N. S.; Schmitt, P. D.; Su, Y.; Liu, Z.; Miller, E.; Variankaval, N.; Marsac, P. J.; Simpson, G. J.; Taylor, L. S. Second harmonic generation microscopy as a tool for the early detection of crystallization in spray dried dispersions. *Journal of Pharmaceutical and Biomedical Analysis* **2017**, *146*, 86–95.

(11) Basso, R. C.; Ribeiro, A. P. B.; Masuchi, M. H.; Gioielli, L. A.; Gonçalves, L. A. G.; dos Santos, A. O.; Cardoso, L. P.; Grimaldi, R. Tripalmitin and monoacylglycerols as modifiers in the crystallisation of palm oil. *Food Chemistry* **2010**, *122*, 1185–1192.

(12) Rodríguez-Hornedo, N.; Nehm, S. J.; Seefeldt, K. F.; Pagan-Torres, Y.; Falkiewicz, C. J. Reaction crystallization of pharmaceutical molecular complexes. *Molecular Pharmaceutics* **2006**, *3*, 362–367.

(13) Sibik, J.; Sargent, M. J.; Franklin, M.; Zeitler, J. A. Crystallization and phase changes in paracetamol from the amorphous solid to the liquid phase. *Molecular Pharmaceutics* **2014**, *11*, 1326–1334.

(14) Sibik, J.; Shalaev, E. Y.; Zeitler, J. A. Glassy dynamics of sorbitol solutions at terahertz frequencies. *Physical Chemistry Chemical Physics* **2013**, *15*, 11931–11942.

(15) Ruggiero, M. T.; Zeitler, J. A. Resolving the origins of crystalline anharmonicity using terahertz time-domain spectroscopy and ab initio simulations. *The Journal of Physical Chemistry B* **2016**, *120*, 11733–11739.

(16) Li, R.; D'Agostino, C.; McGregor, J.; Mantle, M. D.; Zeitler, J. A.; Gladden, L. F. Mesoscopic structuring and dynamics of alcohol/water solutions probed by terahertz time-domain spectroscopy and pulsed field gradient nuclear magnetic resonance. *The Journal of Physical Chemistry B* **2014**, *118*, 10156–10166.

(17) Tielrooij, K.; Paparo, D.; Piatkowski, L.; Bakker, H.; Bonn, M. Dielectric Relaxation Dynamics of Water in Model Membranes Probed by Terahertz Spectroscopy. *Biophysical Journal* **2009**, *97*, 2484–2492.

(18) Tielrooij, K.-J.; Hunger, J.; Buchner, R.; Bonn, M.; Bakker, H. J. Influence of Concentration and Temperature on the Dynamics of Water in the Hydrophobic Hydration Shell of Tetramethylurea. *Journal of the American Chemical Society* **2010**, *132*, 15671–15678.

(19) Zeitler, J. A.; Newnham, D. A.; Taday, P. F.; Strachan, C. J.; Pepper, M.; Gordon, K. C.; Rades, T. Temperature dependent terahertz pulsed spectroscopy of carbamazepine. *Thermochimica Acta* **2005**, *436*, 71–77.

(20) May, R.; Taday, P. F. Crystallization of sucrose monitored by terahertz pulsed spectroscopy. 2013 38th International Conference on Infrared, Millimeter, and Terahertz Waves (IRMMW-THz). 2013; pp 1–1.

(21) Soltani, A.; Gebauer, D.; Duscheck, L.; Fischer, B. M.; Cölfen, H.; Koch, M. Crystallization caught in the act with terahertz Spectroscopy: Non-classical pathway for l-(+)-tartaric acid. *Chemistry* **2017**, *23*, 14128–14132.

(22) Kölbel, J.; Li, Q.; Threlfall, T.; Zeitler, J. A. Measuring the local concentration of semi-crystalline systems with terahertz spectroscopy. *Analytical Chemistry* **2021**, *94*, 1713–1716.

(23) Li, Q.; Kölbel, J.; Threlfall, T.; Zeitler, J. A. Flow cell to study crystallisation processes

in-situ using terahertz time-domain spectroscopy. *IEEE Transactions on Terahertz Science and Technology* **2021**, 1–1.

(24) Macrae, C. F.; Sovago, I.; Cottrell, S. J.; Galek, P. T.; McCabe, P.; Pidcock, E.; Platings, M.; Shields, G. P.; Stevens, J. S.; Towler, M., et al. Mercury 4.0: From visualization to analysis, design and prediction. *Journal of Applied Crystallography* **2020**, *53*, 226–235.

(25) Weil, M. The high-temperature modification of magnesium sulfate (β-MgSO4) from single-crystal data. *Acta Crystallographica Section E: Structure Reports Online* **2007**, *63*, i172–i172.

(26) Hawthorne, F.; Groat, L.; Raudsepp, M.; Ercit, T. Kieserite, $Mg(SO_4)(H_2O)$, a titanite-group mineral. *Neues Jahrbuch für Mineralogie Abhandlungen* **1987**, *157*, 121–132.

(27) Ferraris, G.; Jones, D. W.; Yerkess, J. Refinement of the crystal structure of magnesium sulphate heptahydrate (epsomite) by neutron diffraction. *Journal of the Chemical Society, Dalton Transactions* **1973**, 816–821.

(28) Dovesi, R.; Erba, A.; Orlando, R.; Zicovich-Wilson, C. M.; Civalleri, B.; Maschio, L.; Rérat, M.; Casassa, S.; Baima, J.; Salustro, S., et al. Quantum-mechanical condensed matter simulations with CRYSTAL. *Wiley Interdisciplinary Reviews: Computational Molecular Science* **2018**, *8*, e1360.

(29) Vilela Oliveira, D.; Laun, J.; Peintinger, M. F.; Bredow, T. BSSE-correction scheme for consistent gaussian basis sets of double-and triple-zeta valence with polarization quality for solid-state calculations. *Journal of Computational Chemistry* **2019**, *40*, 2364–2376.

(30) Becke, A. D. A new mixing of Hartree–Fock and local density-functional theories. *The Journal of Chemical Physics* **1993**, *98*, 1372–1377.

(31) Lee, C.; Yang, W.; Parr, R. G. Development of the Colle-Salvetti correlation-energy formula into a functional of the electron density. *Physical Review B* **1988**, *37*, 785.

(32) Grimme, S.; Antony, J.; Ehrlich, S.; Krieg, H. A consistent and accurate ab initio parametrization of density functional dispersion correction (DFT-D) for the 94 elements H-Pu. *The Journal of Chemical Physics* **2010**, *132*, 154104.

(33) Grimme, S.; Ehrlich, S.; Goerigk, L. Effect of the damping function in dispersion corrected density functional theory. *Journal of Computational Chemistry* **2011**, *32*, 1456–1465.

(34) Grimme, S.; Hansen, A.; Brandenburg, J. G.; Bannwarth, C. Dispersion-corrected mean-field electronic structure methods. *Chemical Reviews* **2016**, *116*, 5105–5154.

(35) Axilrod, B.; Teller, E. Interaction of the van der Waals type between three atoms. *The Journal of Chemical Physics* **1943**, *11*, 299–300.

(36) Muto, Y. Force between nonpolar molecules. *Proceedings of the Physico-Mathematical Society of Japan* **1943**, *17*, 629–631.

(37) Donà, L.; Brandenburg, J.; Bush, I.; Civalleri, B. Cost-effective composite methods for large-scale solid-state calculations. *Faraday Discussions* **2020**, *224*, 292–308.

(38) Pascale, F.; Zicovich-Wilson, C. M.; López Gejo, F.; Civalleri, B.; Orlando, R.; Dovesi, R. The calculation of the vibrational frequencies of crystalline compounds and its implementation in the CRYSTAL code. *Journal of Computational Chemistry* **2004**, *25*, 888–897.

(39) Zicovich-Wilson, C.; Pascale, F.; Roetti, C.; Saunders, V.; Orlando, R.; Dovesi, R. Calculation of the vibration frequencies of α-quartz: The effect of Hamiltonian and basis set. *Journal of Computational Chemistry* **2004**, *25*, 1873–1881.

(40) Zalkin, A.; Ruben, H.; Templeton, D. The crystal structure of cobalt sulfate hexahydrate. *Acta Crystallographica* **1962**, *15*, 1219–1224.

(41) Ruggiero, M. T. Invited Review: Modern Methods for Accurately Simulating the Terahertz Spectra of Solids. *Journal of Infrared, Millimeter, and Terahertz Waves* **2020**, *41*.

(42) Fortes, A. D.; Wood, I. G.; Alfredsson, M.; Vocadlo, L.; Knight, K. S. The thermoelastic properties of $MgSO_4 \cdot 7D_2O$ (epsomite) from powder neutron diffraction and ab initio calculation. *European Journal of Mineralogy* **2006**, *18*, 449–462.

(43) Leitner, D. M.; Gruebele, M.; Havenith, M. Solvation dynamics of biomolecules: modeling and terahertz experiments. *HFSP Journal* **2008**, *2*, 314–323.

TOC Graphic

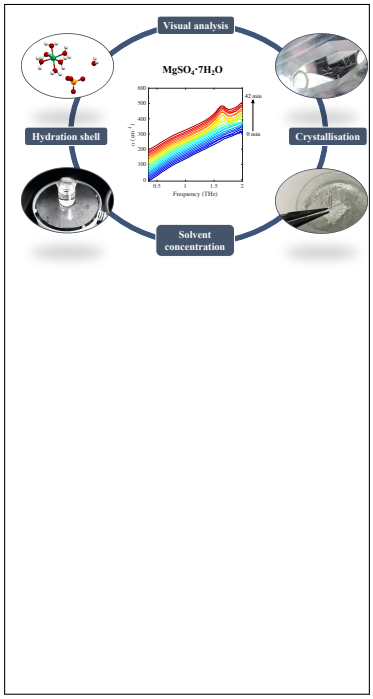
Visual analysis
MgSO4·7H2O
Hydration shell
Crystallisation
Solvent concentration